

CuSbS₂ Nanobricks as Electrode Materials for Lithium Ion Batteries

Zhian Zhang^{1,2}, Chengkun Zhou¹, Yike Liu¹, Jie Li^{1,2}, Yanqing Lai^{1,2}, Ming Jia^{1,2,*}

¹School of Metallurgical Science and Engineering, Central South University, Changsha Hunan 410083, China

²Engineering Research Center of High Performance Battery Materials and Devices, Research Institute of Central South University in Shenzhen, Shenzhen, 518057

*E-mail: csulightmetals11@163.com

Received: 7 May 2013 / Accepted: 13 June 2013 / Published: 1 July 2013

CuSbS₂ nanobricks are prepared via a hot injection method (a fast homogeneous nucleation reaction) by introducing oleylamine (OLA) as surfactant. The phase of each sample was characterized by X-ray diffraction (XRD), and scanning electron microscopy (SEM), transmission electron microscope (TEM) revealed brick-liked nanomaterials were obtained, with a size of 50-200 nm long, 20-50 nm wide, about 10 nm thick. The electrochemical performance was also tested with 2025-type coin cell, and it exhibited a high initial capacity with discharge and charge capacities of 1090 mAh g⁻¹ and 761.6 mAh g⁻¹ respectively, although the capacity retention was insufficient. By using cyclic voltammogram (CV), *ex situ* XRD, the reaction mechanism of the new CuSbS₂ electrode was also examined during the first cycle. In addition, the Electrochemical impedance spectra (EIS) was recommended to study the change in the internal impedance upon cycling.

Keywords: CuSbS₂ nanobricks; Hot injection method; Electrochemical performance; Lithium ion batteries

1. INTRODUCTION

Lithium ion batteries are widely improved and have conquered the portable electronic markets basically. But they still fall short of meeting the demands dictated by the powering of both hybrid electric vehicles and electric vehicles or by the storage of renewable energies (wind, solar), which requires a innovation in the field of active materials of lithium ion batteries [1, 2].

Among the various candidate active materials for secondary lithium ion batteries, metal sulfides are known to be promising materials because of their high theoretical capacity. Binary

sulfides, such as TiS_2 [3], NiS [4], FeS_2 [5], CuS [6], MoS_2 [7,8] and SnS_2 [9], have been considered as electrode materials in lithium ion batteries. Identically, ternary sulfides, like copper-based multicomponent chalcogenides (CBMC), have also attracted considerable attention in recent years due to their potential applications in the energy-related devices. For instance, B. Qu and his co-workers synthesized a ternary Cu_2SnS_3 cabbage-like nanostructures as electrode materials in lithium ion batteries, which showed an initial reversible capacity of 842 mAh g^{-1} and still retained 621 mAh g^{-1} after 50 cycles [10]. The electrochemical performance of CuInS_2 nanocomposite was also investigated by W. Zhang et al., in which hollow nanospheres delivered an initial discharge capacity of 1144 mAh g^{-1} and exhibited good cycle performance with a discharge capacity of 265 mAh g^{-1} after 20 cycles [11]. As an important member of the CBMC family, the ternary $\text{Cu}_x\text{Sb}_y\text{S}_z$ system is made up of four compounds (Cu_3SbS_4 , CuSbS_2 , Cu_3SbS_3 and $\text{Cu}_{12}\text{Sb}_4\text{S}_{13}$), which is widely used in photovoltaic devices and solar cells due to their excellent semiconductor properties [12-14], however, to the best of our knowledge, there is no report on the possible application as active material for lithium ion batteries.

Traditionally, CuSbS_2 , the key part of ternary $\text{Cu}_x\text{Sb}_y\text{S}_z$ system, was synthesized by melting the stoichiometric ratio of the component elements in sealed silica tubes in nitrogen atmosphere [15]. But now various morphologies of CuSbS_2 have been synthesized by solution-based methods. Xie and co-workers have prepared CuSbS_2 nanocrystals in ethylenediamine solution under solvothermal conditions and C. An et al. also successfully obtained CuSbS_2 nanorods via a surfactant-assisted hydrothermal synthesis route [16, 17].

Herein, we obtain a CuSbS_2 nanobricks by employing a hot injection method, based on the reactions between Copper (II) acetylacetonate and antimony(III) acetate and sulfur, respectively. which is a facile approach to nanomaterials [13, 18]. The electrochemical performance of the novel ternary CuSbS_2 as electrode materials for lithium ion batteries was first to be investigated, and the results of electrochemical tests show a high initial lithium ion storage capacity of 1090 mAh g^{-1} , suggesting a promising electrode material for lithium ion batteries.

2. EXPERIMENTAL

2.1. Materials preparation

Copper (II) acetylacetonate ($\text{Cu}(\text{acac})_2$, 97%), antimony(III) acetate ($\text{Sb}(\text{Ac})_3$, 98%), oleylamine (OLA, C-18 content 80%-90%) and sulfur (S, 99.99%) were purchased from Aladdin. Toluene, ethanol were obtained from commercial sources, all chemicals were used without further purification.

All experiments were carried out utilizing hot injection method on a standard air-inert Schlenk line. Typically, 1.5 mmol $\text{Cu}(\text{acac})_2$, 1.5 mmol $\text{Sb}(\text{Ac})_3$, and 12 mL OLA were loaded into a three-neck flask with a capacity of 100 mL, respectively. Then the mixture was heated to approximately 140°C under vacuum and stirring, for degassing about 1h and purging with Ar three times. Here the color of the mixture turned from blue into red-brown. After that, the flask was raised to 260°C and 3 mL of 1M solution of sulfur in OLA were injected into it quickly with the reaction time was last for 1 h.

Upon injection the solution immediately turned into black indicating the rapid nucleation of CuSbS_2 nanobricks. The mixture was then cooled to approximately 70°C by air quenching. The black precipitate was purified with toluene and ethanol for three times, and then large amount of ethanol were added to be washed for another twice, finally dried at 60°C for 8 h in a vacuum oven.

2.2. Materials characterization

The crystal structures of the products were confirmed by X-ray powder diffraction (XRD; Rigaku D/max Diffraction System, $\text{Cu K}\alpha$ radiation $\lambda = 1.5406 \text{ \AA}$). Scanning electron microscope (SEM; FEI Quanta-200), field emission scanning electron microscope (FESEM; Nova NanoSEM 230) and transmission electron microscope (TEM; JEM-2100F) were used for morphology and structure characterization.

2.3. Electrochemical Measurements

For an electrochemical evaluation of CuSbS_2 nanobricks, the electrodes consisted of active materials (80wt.%), carbon black (Super P, 10 wt.%) as a conducting agent and polyvinylidene fluoride (PVdF, 10 wt.%) dissolved in N-methyl pyrrolidinone (NMP) as a binder. Prepared slurries were coated on the copper foil substrates, pressed and dried at 120°C for 8 h under vacuum. The electrodes were assembled into CR2025 coin-type cells with Li electrode and electrolyte (1 M LiPF_6 in EC: EMC: DMC = 1: 1: 1 in volume) in an Ar-filled glove box. The charge-discharge measurements were performed at room temperature with a Land CT2001A battery test system. The cyclic voltammogram (CV) tests were performed with a scanning rate of 0.5 mV s^{-1} between 0.01 V and 3.00 V on a PARSTAT 2273 electrochemical Workstation (PerkinElmer Instrument USA). The Electrochemical impedance spectra (EIS) were recorded on the same instrument in the frequency range 100 kHz-10 mHz.

3. RESULTS AND DISCUSSION

3.1 Structural characterization

The phase and structures of the as-prepared samples are characterized by XRD analysis as shown in Fig. 1. All the identified peaks are labeled and can be readily indexed to a pure orthorhombic phase chalcostibite (CuSbS_2) with cell constants of $a = 6.016 \text{ \AA}$, $b = 3.797 \text{ \AA}$, $c = 14.499 \text{ \AA}$, which are in good agreement with the standard JCPDS card No.88-0288 as well as with existing reports on the orthorhombic chalcostibite [14, 19]. The sharp diffraction peaks indicate that the products are highly crystalline.

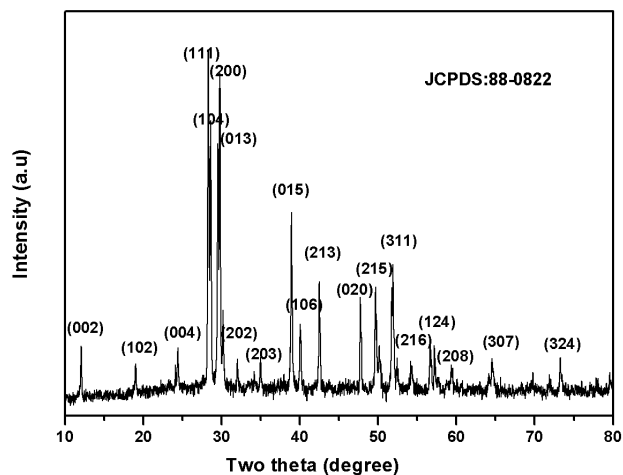


Figure 1. (a) XRD pattern of the as-synthesized CuSbS_2 nanobricks.

3.2 Morphological characterization

In addition to XRD results, the morphology of the as-synthesized products are first characterized by SEM. As revealed in Fig. 2a, the products consist of a large quantity of brick-like structures with a length of several nanometers. The structural features of CuSbS_2 nanobricks are further elucidated by TEM analysis. It is depicted in Fig. 2b and Fig. 2c that a novel cuboid shape (50-200 nm in length, 20-50 nm in width, about 10 nm in thickness) was obtained, which is well consistent with the SEM observation. Therefore, both XRD and TEM analyses manifest that pure CuSbS_2 nanoparticles is successfully synthesized by the present hot injection strategy.

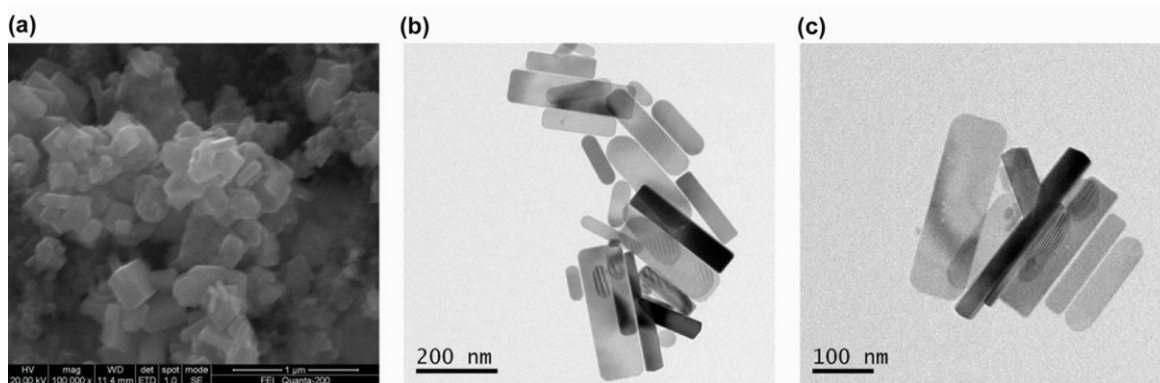


Figure 2. (a) SEM image of CuSbS_2 nanobricks; (b) and (c) TEM images of brick-like CuSbS_2 in different magnification.

3.3 Electrochemical properties

We next investigate the electrochemical performance of the CuSbS_2 nanobricks, and the initial galvanostatic charge-discharge cycle in the potential region of 0.01-3.00 V at a current density of 100 mA g^{-1} is shown in the Fig. 3a along with the selected charge-discharge profiles. The initial discharge

curve shows a relatively flat plateau at about 1.5 V and followed by two small slopes at about 0.75 V and 0.6V with a specific discharge capacity of 1090 mAh g⁻¹, which is much larger than the single Sb₂S₃ electrode [20]. On other hand, the first charge process also reveals two sloping region near 1.1 V and 1.75 V with a specific charge capacity of 761.6 mAh g⁻¹, and the initial coulombic efficiency of 69.9 %. And in the second cycle, the charge and discharge profiles remain generally identical with the initial curve, which illustrates the impedance of the lithium ion batteries could keep stable along with the cycling process. The cycling performance of the Li/CuSbS₂ cell is also revealed in Fig. 3b. We discover that the specific capacity of active materials faded rapidly with a discharge capacity of 85.7 mAh g⁻¹ after 50 cycles, however, the coulombic efficiency could keep stable near 100 %. The obvious capacity decay in the process of cycling may be caused by the complicate irreversible reactions or the pulverization of electrode materials [20, 21].

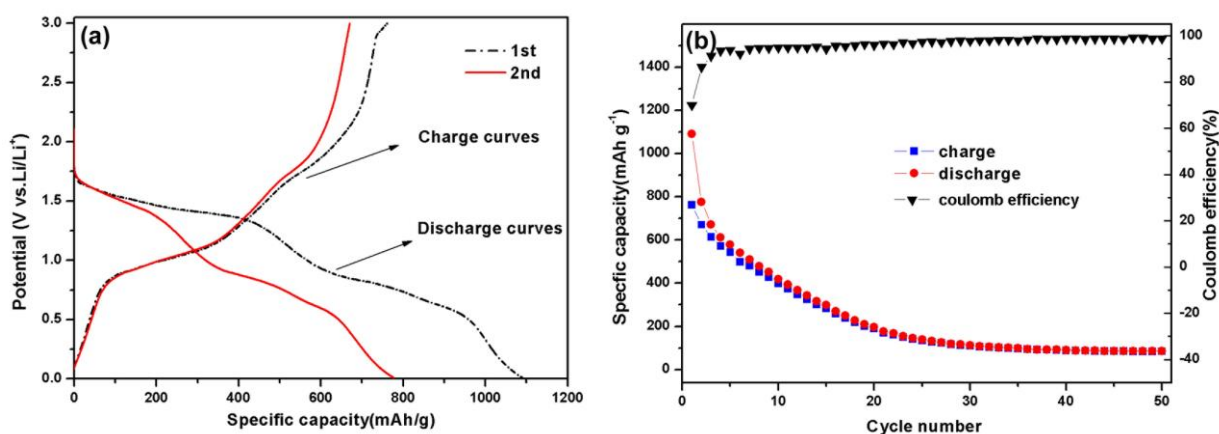


Figure 3. (a) The discharge-charge curves of CuSbS₂ nanobricks; (b) cycling performance and coulombic efficiency of CuSbS₂ electrode.

To better understand the mechanism of the electrochemical reactions in CuSbS₂ electrode, cyclic voltammogram (CV) profiles of the first and second cycle are shown in Fig. 4. The peaks suggest that the ternary CuSbS₂ brick-liked nanostructure electrode involves at least two electrochemical reactions, which is similar to the ternary sulphides by B. Qu et al.'s reported [22]. A sharp peak at ~1.2 V accompanied by two small humps between 0.5 V and 0.75 V are observed in the first cathodic scan (insertion of Li⁺), While in the anodic scan (extraction of Li⁺) exhibits a relatively sharp peak at ~1.15 V followed by a small shoulder at ~1.75 V. In the second cycle, the reductive peak near 1.2 V is much lower than the initial one, suggesting a irreversible reaction may exist in this position, which is the main reason of capacity fading, but the other peaks still remain with just slight shift. The CV analysis is in excellent agreement with the result obtained from charge-discharge curves.

Additionally, the *ex situ* XRD on CuSbS₂ were performed on the electrodes after discharged and charged at selected voltages as shown in Fig. 5. The cells were dismantled inside the glovebox, and then washed the electrodes with solvent DMC to remove the electrolyte. For comparison, XRD pattern of the fresh electrode is also included (Fig. 5a). After the first discharging to 1.00 V, the

diffraction peaks (\blacklozenge) of CuSbS_2 are disappeared gradually while the peaks at $2\theta=27^\circ$, 30.15° and 42° emerge, it means that the CuSbS_2 has decomposed into Sb nanoparticles and Li_2S (Fig. 5b), Upon further discharging to 0.65 V, a new peak emerges at about $2\theta=45.5^\circ$ could be detected, and then discharging to 0.01V, this peak becomes stronger, which is most likely due to the formation of Li_3Sb (Fig. 5c and d). But the peaks of Li_3Sb become weaker when cell charging to 1.2 V, which suggests that the Li_3Sb phase has decomposed, as shown in Fig. 5e. It seems that Li_3Sb are disappeared completely upon charging to 3.00 V (Fig. 5f), and no diffraction peaks of CuSbS_2 could be detected once again by XRD, either. Herein, we deduce that the pair of redox peaks at about 1.15 V/0.75 V in the CV profiles is associated closely with the alloying and dealloying reaction between Li and Sb, which is in good agreement with Sb_2S_3 electrode [20, 23].

Consequently, based on the CV and *ex situ* XRD results, we reckoned that the electrochemical reaction mechanism of CuSbS_2 with lithium involving the following steps is proposed.

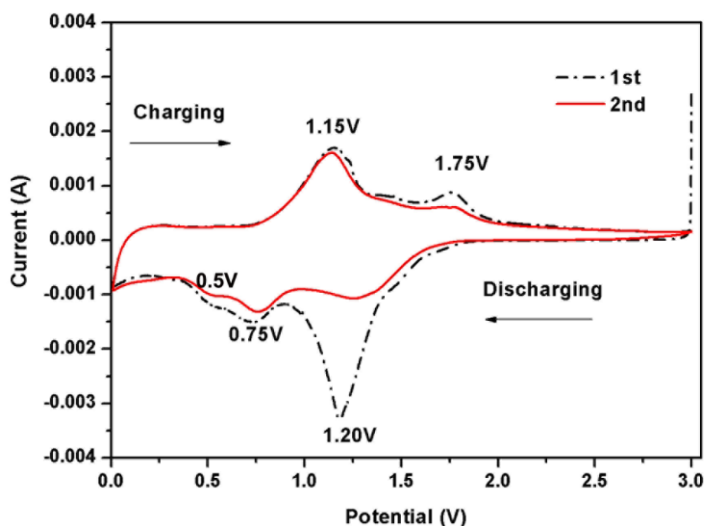
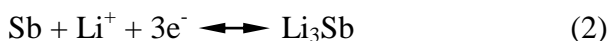


Figure 4. CV profiles of the CuSbS_2 electrode in the first two cycles at 0.5 mV s^{-1} between 3.00 V and 0.01 V.

Fig. 6 shows FESEM images of the as-prepared, lithiated and delithiated CuSbS_2 electrodes during the first cycle. The as-prepared CuSbS_2 electrode exhibits a well-defined surface texture and is composed of very small crystalline grains (Fig. 6a). In addition, some particles agglomerates can be reviewed from FESEM images, this phenomenon is also observed in some metal oxide and nitride electrodes. A clear difference of surface morphologies before and after lithiation of electrodes is apparent (Fig. 6b). When the electrode discharge to 0.01 V, many cracks emerge on the surface and the small crystalline grains is disappeared following with more agglomerates, the morphology change of CuSbS_2 electrode after lithiation should be related to the initial discharge behaviors and the cracks of CuSbS_2 electrode may be closely associated with the alloying and dealloying between Li and Sb, which

had been demonstrated with the *ex situ* XRD [24, 25]. After the first charging to 3.00 V, the cracks still exist (Fig. 6c), the cracks between the as-prepared and after charging to 3.00 V may be related to the origin of the capacity fading of the Li/CuSbS₂ cell.

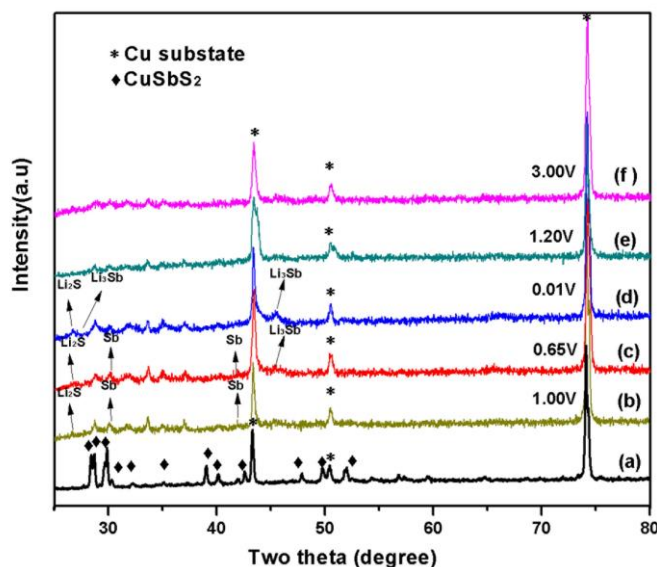


Figure 5. *Ex situ* XRD of the CuSbS₂ electrodes at various states during the first cycle of Li/CuSbS₂ cell; (a) the as-prepared; (b) discharging to 1.00 V; (c) discharging to 0.65 V; (d) discharging to 0.01 V; (e) charging to 1.2 V; (f) charging to 3.00 V..

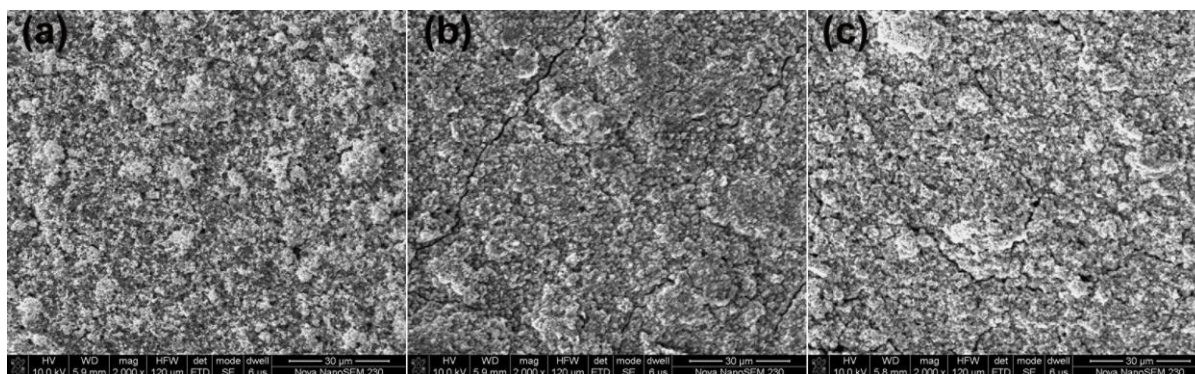


Figure 6. FESEM images of the CuSbS₂ electrodes (a) as-prepared; (b) after the first discharging to 0.01 V; (c) after the first charging to 3.00 V.

In addition, we have studied the change in the internal impedance upon cycling. Electrochemical impedance spectroscopy (EIS) has been carried out in the frequency range of 100 kHz-10 mHz on a cell in as-assembled condition and after 10, 20, 30, 50 cycles, and the corresponding Nyquist plots are shown in Fig. 7. The impedance data for the cell in different cycles all show only one semicircle in the high frequency region with a straight sloping lines in the low frequency region,

respectively. The data have been fitted by Z-View software using equivalent circuit models as reflected in inset of Fig. 7. For the as-assembled cell, the electrolyte resistance (R_s) and the charge transfer resistance (R_{ct}) are found to be 4.05Ω and 156.1Ω , respectively. The fact reflects the poor conductivity of Li/CuSbS₂ battery, which suggests the difficulty of the Li⁺ insertion process. The trend of semicircles' diameter shows the impedance initially decreases and gradually increases upon further cycling with charge transfer resistance (R_{ct}) are 137.6Ω , 140.2Ω , 161.3Ω , 224.9Ω after 10, 20, 30, 50 cycles, respectively. The decreasing of impedance in the initial cycling stage was likely due to the activation of the electrode surface and the appearance of Cu element onto electrode's surface and in the electrolyte [10, 26, 27], which could improve the electrical conductivity. While the subsequent continuous increasing in impedance may be caused by the increasingly serious volume changes associating with the formation of Li₃Sb [24].

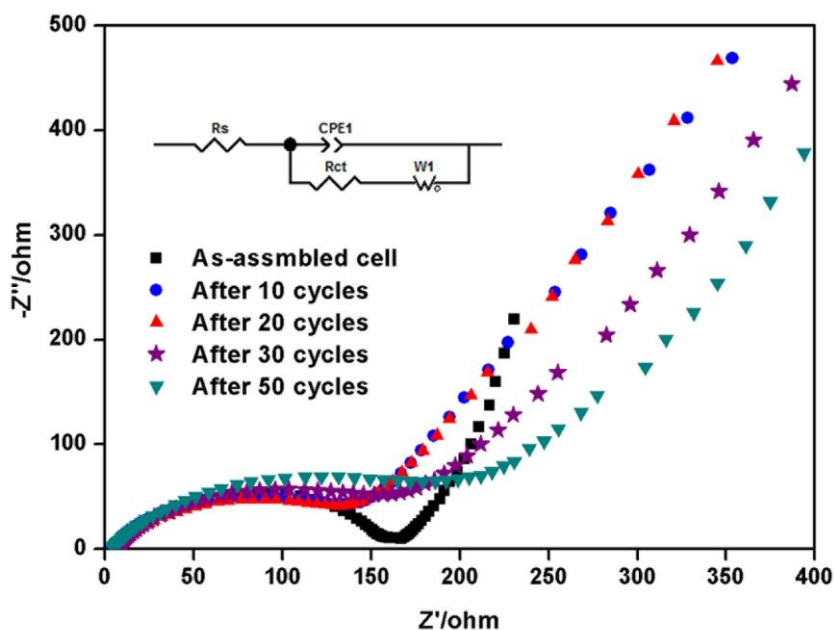


Figure 7. Nyquist plots of CuSbS₂ after different cycling numbers from EIS and the equivalent circuit model (inset).

4. CONCLUSIONS

In summary, brick-liked nanomaterials, CuSbS₂, were prepared by a facile hot injection route, which compose of a large number of cuboid structures. The synthesized CuSbS₂ was first investigated in lithium ion batteries which displayed superior Li storage performances at initial charge-discharge cycle but poor cycle ability with only a capacity of 85.7 mAh g^{-1} retained after 50 cycles. Therefore, further research on improving the cycle performance of ternary CuSbS₂ electrode is still needed. In addition, the results of the communication may stimulate investigation on other copper antimony sulfides such as Cu₃SbS₄, Cu₃SbS₃ etc. as prospective electrode materials.

ACKNOWLEDGEMENTS

The authors acknowledge the financial support of the Strategic Emerging Industries Program of Shenzhen, China (JCYJ20120618164543322) and the National Natural Science Foundation of China (20803095). We also appreciate the support of the Engineering Research Center of Advanced Battery Materials, the Ministry of Education, China.

References

1. J. -M. Tarascon, M. Armand, *Nature*, 414 (2001) 359.
2. J. -M. Tarascon, *Phil. Trans. R. Soc. A*, 368 (2010) 3227.
3. B. M. L. Rao, J. A. Shropshire, *J. Electrochem. Soc.*, 128 (1981) 942.
4. J. Wang, S. Y. Chew, D. Wexler, G. X. Wang, S. H. Ng, S. Zhong, H. K. Liu, *Electrochem. Commun.*, 9 (2007) 1877.
5. Y. S. Horn, Q. -C. Horn, *Electrochim. Acta*, 46 (2001) 2613.
6. J. -S. Chung, H. -J. Sohn, *J. Power Sources*, 108 (2002) 226.
7. C. Zhang, H. B. Wu, Z. Guo, X. W. Lou, *Electrochem. Commun.*, 20 (2012) 7.
8. H. Hwang, H. Kim, J. Cho, *Nano Lett.*, 11 (2011) 4826.
9. J. Seo, J. Jang, S. Park, C. Kim, B. Park, J. Cheon, *Adv. Mater.*, 20(2008) 4269.
10. B. Qu, H. Li, M. Zhang, L. Mei, L. Chen, Y. Wang, Q. Li, T. Wang, *Nanoscale*, 3 (2011) 4389.
11. W. Zhang, H. Zeng, Z. Yang, Q. Wang, *J. Solid State Chem.*, 186 (2012) 58.
12. C. Tablero, *Sol. Energy Mater. Sol. Cells*, 104 (2012) 180.
13. J. Embden, Y. Tachibana, *J. Mater. Chem.*, 22 (2012) 11466.
14. D. J. Temple, A. B. Kehoe, J. P. Allen, G. W. Watson, D. O. Scanlon, *J. Phys. Chem. C*, 116 (2012) 7334.
15. J. H. Wernick, K. E. Benson, *J. Phys. Chem. Solids*, 3 (1957) 157.
16. H. Su, Y. Xie, S. Wan, B. Li, Y. Qian, *Solid State Ionics*, 123 (1999) 319.
17. C. An, Q. Liu, K. Tang, Q. Yang, X. Chen, *J. Cryst. Growth*, 256 (2003) 128.
18. Q. Tian, K. Tao, W. Li, K. Sun, *J. Phys. Chem. C*, 115 (2011) 22886.
19. J. Zhou, G. Q. Bian, Q. Y. Zhu, Y. Zhang, C. Y. Li, J. Dai, *J. Solid State Chem.*, 182 (2009) 259.
20. C. M. Park, Y. Hwa, N. E. Sung, H. J. Sohn, *J. Mater. Chem.*, 20 (2010) 1097.
21. H. Jung, C. -M. Park, H. -J. Sohn, *Electrochim. Acta*, 56 (2011) 2135.
22. B. Qu, M. Zhang, D. Lei, Y. Zeng, Y. Chen, L. Chen, Q. Li, Y. Wang, T. Wang, *Nanoscale*, 3 (2011) 3646.
23. P. V. Prikhodchenko, J. Gun, S. Sladkevich, A. A. Mikhaylov, O. Lev, Y. Y. Tay, S. K. Batabyal, D. Y. W. Yu, *Chem. Mater.*, 24 (2012) 4750.
24. M. M. Thackeray, J. T. Vaughey, C. S. Johnson, A. J. Kropf, R. Benedek, L. M. L. Fransson, K. Edstrom, *J. Power Sources*, 113 (2003) 124.
25. M. Kunda, S. Mahanty, R. N. Basu, *Electrochem. Commun.*, 11 (2009) 1389.
26. J. W. Kim, J. H. Ryu, K. T. Lee, S. M. Oh, *J. Power Sources*, 147 (2005) 227.
27. L. Xue, Z. Fu, Y. Yao, T. Huang, A. Yu, *Electrochim. Acta* 55 (2010) 7310.